

# Study of the $B_s^0 \rightarrow J/\psi \phi$ decay in pp collisions at $\sqrt{s} = 7$ TeV with the CMS detector

G. Cerizza

Department of Physics and Astronomy, University of Tennessee, Knoxville, TN, USA

B-hadrons are an ideal tool for advancing our current understanding of the flavor sector of the Standard Model (SM). The study of B-meson production and decays is one of the key physics themes at the Large Hadron Collider (LHC) thanks to the large production rate and the fact that B-hadrons are relatively easy to trigger on and identify due to their long lifetime and decays to muons. This talk presents the cross section measurement for the exclusive final state  $B_s^0 \rightarrow J/\psi \phi$  and an evaluation of the decay branching fraction from the previously published exclusive-B production cross sections. Besides probing the heavy quark properties for the first time at the LHC energy, these measurements are also important tools for understanding and calibrating the detector, giving input for Monte Carlo tuning, and providing results for direct comparison with other experiments.

## 1. Heavy-flavor physics at the CMS experiment

The measurements of differential cross sections for heavy-quark production in high-energy hadronic interactions are critical input for the underlying next-to-leading order (NLO) Quantum Chromodynamics (QCD) calculations [1]. While progress has been achieved in the understanding of heavy-quark production at Tevatron energies [2–10], large theoretical uncertainties remain due to the dependence on the renormalization and factorization scales. Measurements of b-hadron production at the higher energies provided by the LHC represent an important new test of theoretical approaches that aim to reduce the scale dependence of NLO QCD calculations [11, 12]. The Compact Muon Solenoid (CMS) experiment, that covers a rapidity range complementary to the specialised b-physics experiment LHCb [13], recently measured the cross sections for production of  $B^+$  [14] and  $B^0$  [15] in pp collisions at  $\sqrt{s} = 7$  TeV. This talk presents the first measurement of the production of  $B_s^0$ , with  $B_s^0$  decaying into  $J/\psi \phi$ , that adds information to the understanding of b-quark production at this energy. Data and theoretical predictions are compared to NLO predictions of heavy-quark production. The result, combined with the published  $B^+$  and  $B^0$  production cross section measurements, is then used for the evaluation of the  $B_s^0 \rightarrow J/\psi \phi$  branching fraction. The cross section measurement for the  $B_s^0 \rightarrow J/\psi \phi$  decay is only the first part of a longer term program that includes the measurement of the  $B_s$  mesons properties (lifetime and lifetime difference) and CP-violating parameters (CP-even and CP-odd amplitude strenghts and weak phase).

## 2. The CMS detector

A detailed description of the CMS detector can be found elsewhere [16]. The primary components used in this analysis are the silicon tracker and the muon systems. The tracker operates in a 3.8 T axial magnetic field generated by a superconducting solenoid having an internal diameter of 6 m. The tracker consists of three cylindrical layers of silicon pixel detectors complemented by two disks in the forward and backward directions. The radial region between 20 and 116 cm is occupied by several layers of silicon strip detectors in barrel and disk configurations, ensuring at least nine hits in the pseudorapidity range  $|\eta| < 2.4$ , where  $\eta = -\ln[\tan(\theta/2)]$  and  $\theta$  is the polar angle of the track measured from the positive  $z$ -axis of a right-handed coordinate system, with the origin at the nominal interaction point, the  $x$ -axis pointing to the centre of the LHC, the  $y$ -axis pointing up (perpendicular to the LHC plane), and the  $z$ -axis along the counterclockwise-beam direction. An impact parameter resolution of about  $15 \mu\text{m}$  and a  $p_T$  resolution of about 1.5% are achieved for charged particles with transverse momenta up to  $100 \text{ GeV}/c$ . Muons are identified in the range  $|\eta| < 2.4$ , with detection planes made of drift tubes, cathode strip chambers, and resistive plate chambers, embedded in the steel return yoke. The first level of the CMS trigger system uses information from the crystal electromagnetic calorimeter, the brass/scintillator hadron calorimeter, and the muon detectors to select the most interesting events in less than  $1 \mu\text{s}$ . The high level trigger (HLT) employs software algorithms and a farm of commercial processors to further decrease the event rate using information from all detector subsystems. The events used in the measurement reported in this paper were collected with a trigger requiring the presence of two muons at the HLT, with no explicit momentum threshold.

### 3. Muon reconstruction

In CMS muons are defined as tracks reconstructed in the silicon trackers and associated to a compatible signal in the muon chambers. Two different muon types are available in CMS. The first one, referred to as a *Global Muon*, provides high-purity reconstruction for muons with  $p_T > 4$  GeV/c in the central pseudo-rapidity region  $|\eta| < 1.5$ , and  $p_T > 1$  GeV/c in the forward region. *Global Muons* are built as a combined fit of silicon and muon-chamber hits, belonging to independent tracks found in the tracker and muon systems. The second muon type, referred to as a *Tracker Muon*, achieves a better reconstruction efficiency at lower momenta. The requirements for a *Tracker Muon* are relaxed compared to the *Global Muons*, at the expense of a slightly larger background: tracks found in the tracker matched to only one muon segment are accepted and not refitted. If two (or more) tracks are close to each other, it is possible that the same muon segment or set of segments is associated to more than one track. In this case the best track is selected based on the matching between the extrapolated track and the segment in the muon detectors.

### 4. Strategy outline

A sample of exclusive  $B_s^0 \rightarrow J/\psi \phi$  decays, with  $J/\psi \rightarrow \mu^+ \mu^-$  and  $\phi \rightarrow K^+ K^-$ , is reconstructed from the data collected in 2010 by the CMS experiment, corresponding to an integrated luminosity of  $39.6 \pm 1.6 \text{ pb}^{-1}$ . The differential production cross sections,  $d\sigma/dp_T^B$  and  $d\sigma/dy^B$ , are determined as functions of the transverse momentum  $p_T^B$  and rapidity  $|y^B|$  of the reconstructed  $B_s^0$  candidate. Here, the rapidity  $y^B$  is defined as  $\frac{1}{2} \ln \frac{E + cp_L}{E - cp_L}$ , where  $E$  is the particle's energy and  $p_L$  is the particle's momentum along the counterclockwise beam direction. The differential cross sections are calculated from the measured signal yields ( $n_{\text{sig}}$ ), corrected for the overall efficiency ( $\epsilon$ ), bin size ( $\Delta x$ , with  $x = p_T^B, |y^B|$ ), and integrated luminosity ( $L$ ) as

$$\frac{d\sigma(\text{pp} \rightarrow B_s^0 \rightarrow J/\psi \phi)}{dx} = \frac{n_{\text{sig}}}{2 \cdot \epsilon \cdot \mathcal{B} \cdot L \cdot \Delta x}, \quad (1)$$

where  $\mathcal{B}$  is the product of the branching fractions for the decays of the  $J/\psi$  and  $\phi$  mesons. In each bin the signal yield is extracted with an unbinned maximum likelihood fit to the  $J/\psi \phi$  invariant mass and proper decay length  $ct$  of the  $B_s^0$  candidates. The factor of two in Eq. 1 is required since we report the result as a cross section for  $B_s^0$  production alone, while both  $B_s^0$  and  $\bar{B}_s^0$  are included in  $n_{\text{sig}}$ . The size of the bins is chosen such that the statistical uncertainty on  $n_{\text{sig}}$  is comparable in each of them.

#### 4.1. Reconstruction and $B_s^0$ selection

Reconstruction of  $B_s^0 \rightarrow J/\psi \phi$  candidates begins by identifying  $J/\psi \rightarrow \mu^+ \mu^-$  decays. The muon candidates must have one or more reconstructed segments in the muon system that match the extrapolated position of a track reconstructed in the tracker. Furthermore, the muons are required to lie within a kinematic acceptance region defined as:  $p_T^\mu > 3.3$  GeV/c for  $|\eta^\mu| < 1.3$ ; total momentum  $p^\mu > 2.9$  GeV/c for  $1.3 < |\eta^\mu| < 2.2$ ; and  $p_T^\mu > 0.8$  GeV/c for  $2.2 < |\eta^\mu| < 2.4$ . Two oppositely charged muon candidates are paired and are required to originate from a common vertex using a Kalman vertex fit [17]. The muon pair is required to have a transverse momentum  $p_T > 0.5$  GeV/c and an invariant mass within 150 MeV/ $c^2$  of the world average  $J/\psi$  mass value [18], which corresponds to more than three times the measured dimuon invariant mass resolution [19].

Candidate  $\phi$  mesons are reconstructed from pairs of oppositely charged tracks with  $p_T > 0.7$  GeV/c that are selected from a sample with the muon candidate tracks removed. The tracks are required to have at least five hits in the silicon tracker detectors, and a track  $\chi^2$  per degree of freedom less than five. Each track is assumed to be a kaon and the invariant mass of a track pair has to be within 10 MeV/ $c^2$  of the world average  $\phi$ -meson mass [18].

The  $B_s^0$  candidates are formed by combining a  $J/\psi$  candidate with a  $\phi$  candidate. The two muons and the two kaons are subjected to a combined vertex and kinematic fit [20], where in addition the dimuon invariant mass is constrained to the nominal  $J/\psi$  mass. The selected candidates must have a resulting  $\chi^2$  vertex probability greater than 2%, an invariant mass between 5.20 and 5.65 GeV/ $c^2$ , and be in the kinematic range  $8 < p_T^B < 50$  GeV/c and  $|y^B| < 2.4$ . For events with more than one candidate, the one with the highest vertex-fit probability is selected. This results in the correct choice 97% of all cases, as determined from simulated signal events.

The proper decay length of each selected  $B_s^0$  candidate is calculated using the formula  $ct = c(M_B/p_T^B)L_{xy}$ , where the transverse decay length  $L_{xy}$  is the length of the vector  $\vec{s}$  pointing from the primary vertex [21] to the

secondary vertex projected onto the  $B_s^0$  transverse momentum:  $L_{xy} = (\vec{s} \cdot \vec{p}_T^B)/p_T^B$ , with  $M_B$  the reconstructed mass of the  $B_s^0$  candidate. Candidate  $B_s^0$  mesons are accepted within the range  $-0.05 < ct < 0.35$  cm. A total of 6,200 events pass all the selection criteria.

The efficiency of the  $B_s^0$  reconstruction is computed with a combination of techniques using the data and large samples of simulated signal events generated using PYTHIA 6.422 [22]. The decays of unstable particles are described by the EVTGEN [23] simulation. Long-lived particles are then propagated through a detailed description of the CMS detector based on the GEANT4 [24] package. The trigger and muon-reconstruction efficiencies are obtained from a large sample of inclusive  $J/\psi \rightarrow \mu^+ \mu^-$  decays. The total efficiency of this selection, defined as the fraction of  $B_s^0 \rightarrow J/\psi \phi$  decays produced with  $8 < p_T^B < 50$  GeV/c and  $|y^B| < 2.4$  that pass all criteria, ranges from 1.3% for  $p_T^B \approx 8$  GeV/c to 19.6% for  $p_T^B > 23$  GeV/c.

## 4.2. Muon efficiency

The ‘‘Tag and Probe’’ [19] technique is a data driven method to measure the single muon tracking, identification and trigger efficiencies. It makes use of a well-known dimuon resonance (such as  $J/\psi$  mesons) to supply tags and probes. The choice of such resonance is due to the CMS experiment ability to measure muon momenta with high precision and reconstruct and identify muons with high efficiencies. Events are selected with strict selection requirements on one muon (*tag*), and with a more relaxed selection on the other track (*probe*), such that the selection applied to the probe track does not bias the efficiency that one wants to measure. The *probe* tracks are separated into two categories depending on whether they pass or fail the more restrictive selection. If  $p_{tag}$  and  $p_{probe}$  are the four-momenta of the *tag* muon and *probe* track respectively then the invariant mass  $m$  of the particle is given by:

$$m = \sqrt{p_{tag}^2 + p_{probe}^2} \quad (2)$$

The technical chain runs as follows: all events of the  $J/\psi$  samples are passed through. An event is kept if a tag muon + probe track combination is found while satisfying the predefined criteria. In this case the invariant mass of the combination enters a muon-track mass histogram. The criteria for the choice of both, *tag* and *probe*, should be defined such that background is reduced and the  $J/\psi$  mass peak is clearly visible. If the track is subsequently identified as a global/tracker muon the invariant mass of the tag and probe combination enters another muon-muon mass histogram. The latter should contain almost exclusively  $J/\psi \rightarrow \mu^+ \mu^-$  events. A simultaneous unbinned Maximum Likelihood (ML) fit to both mass distribution extracts the efficiency. The dimuon efficiencies are calculated as the product of the single-muon efficiencies obtained with this method. Corrections to account for correlations between the two muons (1–3%) are obtained from simulation studies. The correction factors are determined in bins of single muon  $p_T^\mu$  and  $\eta^\mu$ , and are applied independently to each muon from a  $B_s^0 \rightarrow J/\psi \phi$  decay in the simulation to determine the total corrected efficiency.

## 5. Fit technique

The two main background sources are prompt and non-prompt  $J/\psi$  production. The latter background is mainly composed of  $B^+$  and  $B^0$  mesons that decay to a  $J/\psi$  and a higher-mass K-meson state (such as the  $K_1^+$ ). Such events tend to have lower reconstructed  $M_B$  mass. Inspection of the reconstructed  $J/\psi \phi$  invariant mass for a large variety of potential B background channels confirms that there is no single dominant component and that the channel  $B^0 \rightarrow J/\psi K^{*0}$  (with  $K^{*0} \rightarrow K^+ \pi^-$ ), which *a priori* is kinematically similar to the signal decay and more abundantly produced, is strongly suppressed by the restriction on the  $K^+ K^-$  invariant mass. A study of the sidebands of the dimuon invariant mass distribution confirms that the contamination from events without a  $J/\psi$  decay to two muons is negligible after all selection criteria have been applied.

The signal yields in each  $p_T^B$  and  $|y^B|$  bin are obtained using an unbinned extended maximum-likelihood fit to  $M_B$  and  $ct$ . The likelihood for event  $j$  is obtained by summing the product of the yield  $n_i$  and the probability density functions (PDF)  $\mathcal{P}_i$  and  $\mathcal{Q}_i$  for each of the signal and background hypotheses  $i$ . Three individual components are considered: signal, non-prompt  $b \rightarrow J/\psi X$ , and prompt  $J/\psi$ . The extended likelihood function is then the product of likelihoods for each event  $j$ :

$$\mathcal{L} = \exp \left( - \sum_{i=1}^3 n_i \right) \prod_j \left[ \sum_{i=1}^3 n_i \mathcal{P}_i(M_B; \vec{\alpha}_i) \mathcal{Q}_i(ct; \vec{\beta}_i) \right]. \quad (3)$$

The PDFs  $\mathcal{P}_i$  and  $\mathcal{Q}_i$  are parameterized separately for each fit component with shape parameters  $\vec{\alpha}_i$  for  $M_B$  and  $\vec{\beta}_i$  for  $ct$ . The yields  $n_i$  are then determined by minimizing the quantity  $-\ln\mathcal{L}$  with respect to the signal yields and a subset of the PDF parameters [26]. The PDFs are constructed from basic analytical functions that satisfactorily describe the variable distributions from simulated events. Shape parameters are obtained from data when possible. The  $M_B$  PDF is the sum of two Gaussian functions for the signal, a second-order polynomial for the non-prompt  $J/\psi$  that allows for possible curvature in the shape, and a first-order polynomial for prompt  $J/\psi$ . The resolution on  $M_B$  is approximately 20 MeV/ $c^2$  near the  $B_s^0$  mass.

For the signal, the  $ct$  PDF is a single exponential parameterized in terms of a proper decay length  $c\tau$ . It is convolved with a resolution function that is a combination of two Gaussian functions to account for a dominant core and small outlier distribution; the core fraction is varied in the fit and found to be consistently larger than 95%. The  $ct$  distribution for the non-prompt  $J/\psi$  background is described by a sum of two exponentials, with effective lifetimes that are allowed to be different. The “long-lifetime exponential” corresponds to decays of  $b$ -hadrons to a  $J/\psi$  plus some charged particles that survive the  $\phi$  selection, while the “short-lifetime exponential” accounts for events where the muons from the  $J/\psi$  decay are wrongly combined with hadron tracks originating from the pp collision point. The exponential functions are convolved with a resolution function with the same parameters as the signal. For the prompt  $J/\psi$  component the pure resolution function is used. The core resolution in  $ct$  is measured in data to be 45  $\mu\text{m}$ . All background shapes are obtained directly from data, while the signal shape in  $M_B$  is taken from a fit to reconstructed signal events from the simulation. The effective lifetime and resolution function parameters for prompt and non-prompt backgrounds are extracted from data in regions of  $M_B$  that are separated by more than four times the width of the observed  $B_s^0$  signal from the mean  $B_s^0$  peak position ( $M_B$  sidebands):  $5.20 < M_B < 5.29$  GeV/ $c^2$  and  $5.45 < M_B < 5.65$  GeV/ $c^2$ . A comparison of the PDF shapes for the different sideband regions in simulated events confirms that they are extrapolated well into the signal region. With the lifetimes for signal and non-prompt background fixed from this first step, the resolution function parameters are then determined separately in each  $p_T^B$  and  $|y^B|$  bin, from the  $M_B$  sidebands. The signal and background yields in each  $p_T^B$  and  $|y^B|$  bin are determined in a final iteration, using the full  $M_B$  range, with all parameters floating except the background lifetimes and the lifetime resolution functions, which are fixed to the results of the fit to the  $M_B$  sidebands. It has been verified that leaving all parameters floating changes the signal yield by an amount smaller than the systematic uncertainty assigned to the fit procedure.

## 5.1. Fit results

Figure 1 shows the fit projections for  $M_B$  and  $ct$  from the inclusive sample with  $8 < p_T^B < 50$  GeV/ $c$  and  $|y^B| < 2.4$ . When plotting  $M_B$ , the selection  $ct > 0.01$  cm is applied for better visibility of the individual contributions. The number of signal events in the entire data sample is  $549 \pm 32$ , where the uncertainty is statistical only. The obtained proper decay length of the signal,  $c\tau = 478 \pm 26$   $\mu\text{m}$ , is within 1.4 standard deviations of the world average value [18], even though this analysis was not optimized for lifetime measurements.

## 6. Systematics

The cross section measurement is affected by several sources of systematic uncertainty arising from uncertainties on the fit, efficiencies, branching fractions, and integrated luminosity. In every bin the total uncertainty is about 11%. Uncertainties on the muon efficiencies from the trigger, identification, and tracking are determined directly from data (3–5%). The uncertainty of the method employed to measure the efficiency in the data has been estimated from a large sample of full-detector simulated events (1–3%). The tracking efficiency for the charged kaons is consistent with simulation. A conservative uncertainty of at most 9% in each bin has been assigned for the hadronic track reconstruction (adding linearly the uncertainties on the two kaon tracks [25]), which includes the uncertainty due to misalignment of the silicon detectors. The uncertainty of the fit procedure arising from potential biases and imperfect knowledge of the PDF parameters is estimated by varying the parameters by one standard deviation (2–4%). The contribution related to the  $B_s^0$  momentum spectrum (1–3%) is evaluated by reweighting the shape of the  $p_T^B$  distribution generated with PYTHIA to match the spectrum predicted by MC@NLO [27]. An uncertainty of 1% is assigned to the variation of the selection criteria applied to the vertex fit probability, the transverse momentum of the kaons, the  $B_s^0$  transverse momentum, and the  $K^+K^-$  invariant mass. An uncertainty is added to account for the limited number of simulated events (at most 3% in the highest  $p_T^B$  bin). The total uncorrelated systematic uncertainty in each bin is the sum in quadrature of the individual uncertainties (see Table I). In addition, there are common uncertainties of 4% from the integrated luminosity measurement [28] and 1.4% from the  $J/\psi$  and  $\phi$  branching fractions [18]. As

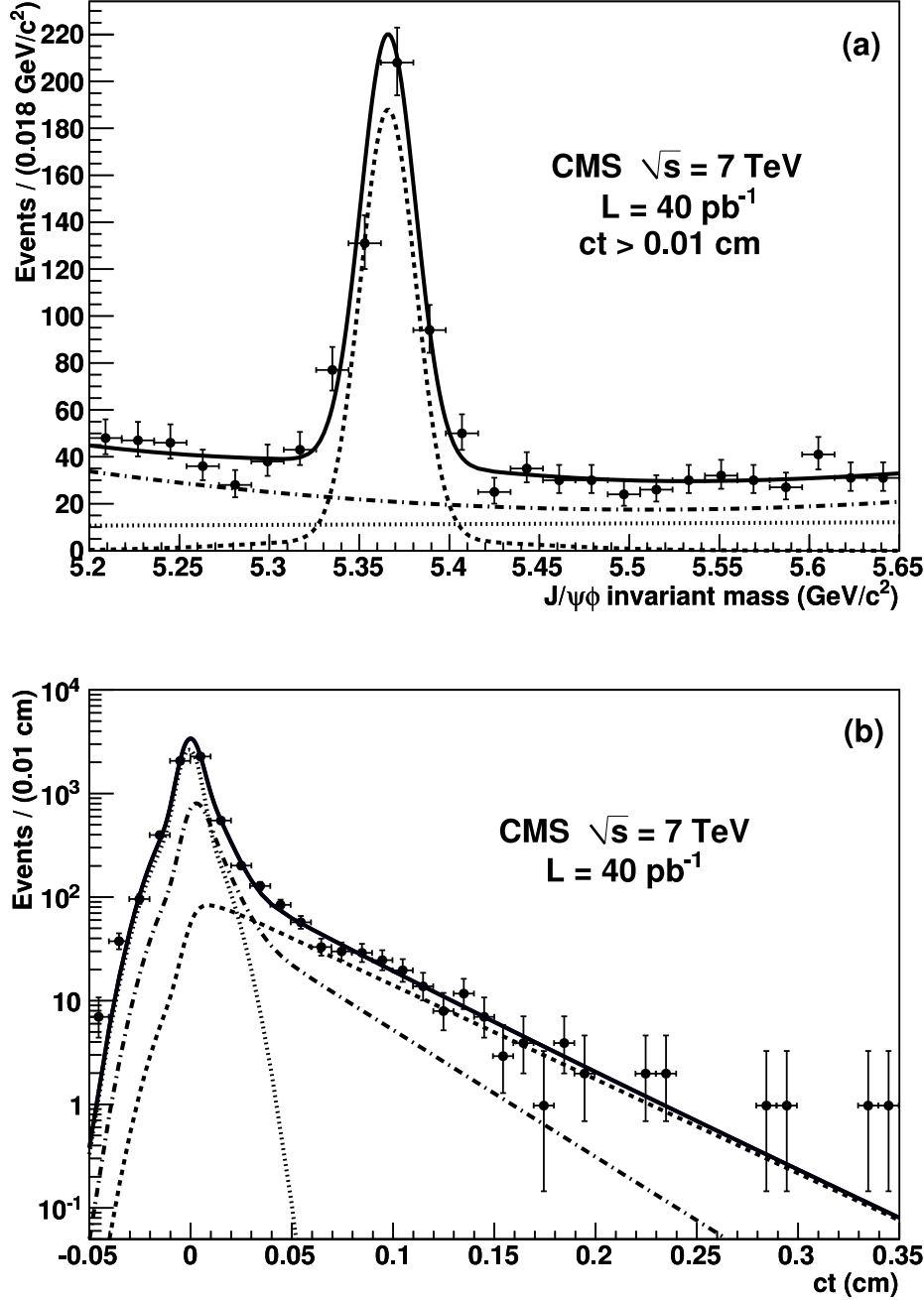


Figure 1: Projections of the fit results in  $M_B$  (a) and  $ct$  (b) for  $8 < p_T^B < 50 \text{ GeV}/c$  and  $|y^B| < 2.4$ . The curves in each plot are: the sum of all contributions (solid line); signal (dashed); prompt  $J/\psi$  (dotted); and non-prompt  $J/\psi$  (dot-dashed). For better visibility of the individual contributions, plot (a) includes the requirement  $ct > 0.01 \text{ cm}$ .

the reported result is a measurement of the  $B_s^0$  cross section times the  $B_s^0 \rightarrow J/\psi \phi$  branching fraction, the 30% uncertainty in the  $B_s^0 \rightarrow J/\psi \phi$  branching fraction [18] is not included in the result.

Table I: Summary table of the relative systematic uncertainties in the measurement of the  $B_s^0 \rightarrow J/\psi \phi$  production cross section.

Source	Uncertainty (%)
Muon Reconstruction Efficiency	3 – 5
Hadron Tracking Efficiency	7.8
Reconstruction Efficiency	2 – 3
Misalignment	2 – 4
$p_T^B -  y^B $ Spectrum	1 – 3
Probability Density Function	2 – 4
Uncorrelated Systematic Errors	10 – 11
Branching Fractions	1.4
Luminosity	4
Correlated Systematic Errors	4.2
Total Systematic Error	11 – 12

## 7. Differential cross section measurement

The differential cross sections times branching fraction as functions of  $p_T^B$  and  $|y^B|$  are plotted in Fig. 2, together with predictions from MC@NLO and PYTHIA. The predictions of MC@NLO use the renormalization and factorization scales  $\mu = \sqrt{m_b^2 c^4 + p_T^2 c^2}$ , where  $p_T$  is the transverse momentum of the b quark, a b-quark mass of  $m_b = 4.75 \text{ GeV}/c^2$ , and the CTEQ6M parton distribution functions [29]. The uncertainty in the MC@NLO cross section is obtained simultaneously varying the renormalization and factorization scales by factors of two, varying  $m_b$  by  $\pm 0.25 \text{ GeV}/c^2$ , and using the CTEQ6.6 parton distribution function set. The prediction of PYTHIA uses the CTEQ6L1 parton distribution functions [29], a b-quark mass of  $4.8 \text{ GeV}/c^2$ , and the Z2 tune [30] to simulate the underlying event. The total integrated  $B_s^0$  cross section times  $B_s^0 \rightarrow J/\psi \phi$  branching fraction for the range  $8 < p_T^B < 50 \text{ GeV}/c$  and  $|y^B| < 2.4$  is measured to be  $(6.9 \pm 0.6 \pm 0.6) \text{ nb}$ , where the first uncertainty is statistical and the second is systematic. The statistical and systematic uncertainties are derived from the bin-by-bin uncertainties and propagated through the sum. The measured total cross section lies between the theoretical predictions of MC@NLO ( $4.6_{-1.7}^{+1.9} \pm 1.4 \text{ nb}$ ) and PYTHIA ( $9.4 \pm 2.8 \text{ nb}$ ), where the last uncertainty is from the  $B_s^0 \rightarrow J/\psi \phi$  branching fraction [18]. Also the previous CMS cross-section measurements of  $B^+$  [14] and  $B^0$  [15] production in pp collisions at  $\sqrt{s} = 7 \text{ TeV}$ , gave values between the two theory predictions, indicating internal consistency amongst the three different B-meson results.

## 8. Evaluation of the branching fraction for $B_s^0 \rightarrow J/\psi \phi$

The branching fraction  $BF(B_s^0 \rightarrow J/\psi \phi)$  can be calculated independently with respect to either the  $B^+ \rightarrow J/\psi K^+$  or the  $B^0 \rightarrow J/\psi K_s^0$  decay channels. The observed cross section for the decay mode  $B_s^0 \rightarrow J/\psi \phi$  can be written as:

$$\sigma(pp \rightarrow B_s^0 \rightarrow J/\psi \phi) = \sigma(pp \rightarrow \bar{b}) \cdot f_s \cdot BF(B_s^0 \rightarrow J/\psi \phi) \cdot f_{kin}^{B_s^0} \quad (4)$$

and similarly, for the  $B^+$  and  $B^0$  mode:

$$\sigma(pp \rightarrow B^+ X) = \sigma(pp \rightarrow \bar{b}) \cdot f_u \cdot f_{kin}^{B^+} \quad (5)$$

$$\sigma(pp \rightarrow B^0 X) = \sigma(pp \rightarrow \bar{b}) \cdot f_d \cdot f_{kin}^{B^0} \quad (6)$$

Here, the  $f_u$ ,  $f_d$ , and  $f_s$  are the probabilities that the b anti-quark will hadronize and form a  $B^+$ ,  $B^0$ , and  $B_s^0$  meson, respectively. The fractions  $f_{kin}^B$  correct for the limited range in rapidity and transverse momentum in the different analyses. The extrapolation to the full kinematic range is theory dependent. The NLO theory predictions [27] for the expected differential cross section [14, 15, 31] values are in good agreement with the measured ones in each of the three decay channels. Therefore, it is possible to identify the best central model (CTEQ6M,  $Q_R = Q_F = 1$ , and  $m_b = 4.75 \text{ GeV}/c^2$ ) to predict the full kinematic range in  $p_T^B$  and  $|y^B|$ . The spectra are obtained from a number of NLO generated events large enough to keep the relative statistical error

Table II: Summary table for the fragmentation fractions used in the evaluation of the  $B_s^0 \rightarrow J/\psi \phi$  branching fraction.

<b>LEP+Tevatron</b>	
$\Gamma(\bar{b} \rightarrow B_s^0)$	$(11.0 \pm 1.2)\%$
$\Gamma(\bar{b} \rightarrow B^+)$	$(40.3 \pm 1.1)\%$
$\Gamma(\bar{b} \rightarrow B^0)$	$(40.3 \pm 1.1)\%$
$\frac{f_s}{f_{u,d}} = \frac{\Gamma(B_s^0)}{\Gamma(B^{+,0})}$	$(27.2 \pm 3.1)\%$
<b>Tevatron</b>	
$\Gamma(\bar{b} \rightarrow B_s^0)$	$(11.1 \pm 1.4)\%$
$\Gamma(\bar{b} \rightarrow B^+)$	$(33.9 \pm 3.1)\%$
$\Gamma(\bar{b} \rightarrow B^0)$	$(33.9 \pm 3.1)\%$
$\frac{f_s}{f_{u,d}} = \frac{\Gamma(B_s^0)}{\Gamma(B^{+,0})}$	$(32.7 \pm 5.1)\%$

on the predicted ratio at 0.1%. The values for the branching fractions are derived from the measured cross sections:

$$\text{BF}(B_s^0 \rightarrow J/\psi \phi) = \frac{\sigma(pp \rightarrow B_s^0 \rightarrow J/\psi \phi)}{\sigma(pp \rightarrow B^{+,0} X)} \cdot \frac{f_{u,d}}{f_s} \cdot \frac{f_{kin}^{B^{+,0}}}{f_{kin}^{B_s^0}} \quad (7)$$

Both values depend on the ratio of the fraction of kinematic ranges that vary slowly over a wide range of model parameters. The values for the fragmentation fractions are obtained from HFAG, printed in PDG [18] under b-hadron admixtures. Both results, from Tevatron and from the combination of LEP and Tevatron measurements, are considered and reported in Table II. The sources of uncertainties are listed in Table III.

 Table III: Summary table of the systematic uncertainties for the evaluation of the  $B_s^0 \rightarrow J/\psi \phi$  branching fraction.

Source	$\text{BF}_{B^+ \rightarrow J/\psi K^+}^{B_s^0 \rightarrow J/\psi \phi}$	$\text{BF}_{B^0 \rightarrow J/\psi K_s^0}^{B_s^0 \rightarrow J/\psi \phi}$
<b>Experimental Uncertainties</b>		
Cross Section	15.8	16.5
NLO Spectrum	4.6	4.3
<b>PDG Uncertainties</b>		
Branching Fractions	3.5	3.8
Fragmentation Fractions	11.2	11.2

The experimental error is the sum in quadrature of the statistical and systematic uncertainties calculated as described in the cross section measurement papers [14, 15, 31]. It contains the uncertainty of the yield as extracted from maximum likelihood fits, the uncertainty on the reconstruction and hadron-tracking efficiencies, misalignment, and the variation with different models to correct for the limited kinematic ranges. From that, we distinguish the uncertainties of the branching fractions and the fragmentation fractions in PDG [18]. Individual uncertainties are added in quadrature. The cross section measurements in the different exclusive B decay modes, omitting the uncertainty due to the luminosity measurement, are:

- $\sigma(pp \rightarrow B_s^0 \rightarrow J/\psi \phi) = (6.9 \pm 0.6 \pm 0.5) \times 10^{-3} \mu\text{b}$
- $\sigma(pp \rightarrow B^+ X) = (28.3 \pm 2.4 \pm 2.0) \mu\text{b}$
- $\sigma(pp \rightarrow B^0 X) = (33.2 \pm 2.5 \pm 3.1) \mu\text{b}$

The branching fraction  $\text{BF}(B_s^0 \rightarrow J/\psi \phi)$  is calculated according to Eq. 7 with respect to the  $B^+$  meson and to the  $B^0$  meson productions. The two measurements of the branching fraction  $\text{BF}(B_s^0 \rightarrow J/\psi \phi)$  overlap within one standard deviation. Their error weighted average is

$$\text{BF}(B_s^0 \rightarrow J/\psi \phi) = (1.8 \pm 0.2 \pm 0.2) \times 10^{-3} \quad (8)$$

where the errors are the combined experimental and PDG uncertainties, respectively. The result is listed in the same way as PDG does for the present world average. The result agrees within one standard deviation with the PDG value [18] of  $\text{BF}(\text{B}_s^0 \rightarrow \text{J}/\psi \phi) = (1.4 \pm 0.4 \pm 0.2) \times 10^{-3}$  assuming the same uncertainty on the b-quark fragmentation fraction. Using the fragmentation fractions as extracted from the Tevatron, only, the error weighted average for the branching fraction is

$$\text{BF}(\text{B}_s^0 \rightarrow \text{J}/\psi \phi) = (1.5 \pm 0.2 \pm 0.2) \times 10^{-3} \quad (9)$$

to be compared with the PDG value  $\text{BF}(\text{B}_s^0 \rightarrow \text{J}/\psi \phi) = (1.2 \pm 0.3 \pm 0.2) \times 10^{-3}$  that has been extracted in the same way.

## 9. Summary

In summary, the first measurements of the  $\text{B}_s^0$  differential cross sections  $d\sigma/dp_T^{\text{B}}$  and  $d\sigma/dy^{\text{B}}$  in pp collisions at  $\sqrt{s} = 7$  TeV and in the decay channel  $\text{B}_s^0 \rightarrow \text{J}/\psi \phi$  have been presented. The measurement has been performed in four bins in the kinematic range  $|y^{\text{B}}| < 2.4$  and  $8 < p_T^{\text{B}} < 50$  GeV/ $c$ . This study complements previous results in moving towards a comprehensive description of b-hadron production at  $\sqrt{s} = 7$  TeV. An estimation of the  $\text{B}_s^0 \rightarrow \text{J}/\psi \phi$  branching fraction has been calculated from the published CMS measurements of inclusive  $\text{B}^+$  and  $\text{B}^0$  production cross section. We calculate the branching fraction for the  $\text{B}_s^0 \rightarrow \text{J}/\psi \phi$  decay, assuming the fragmentation fractions extracted from measurements at the Tevatron, to  $(1.5 \pm 0.2 \pm 0.2) \times 10^{-3}$  that agrees within one standard deviation with the value published from the Tevatron.



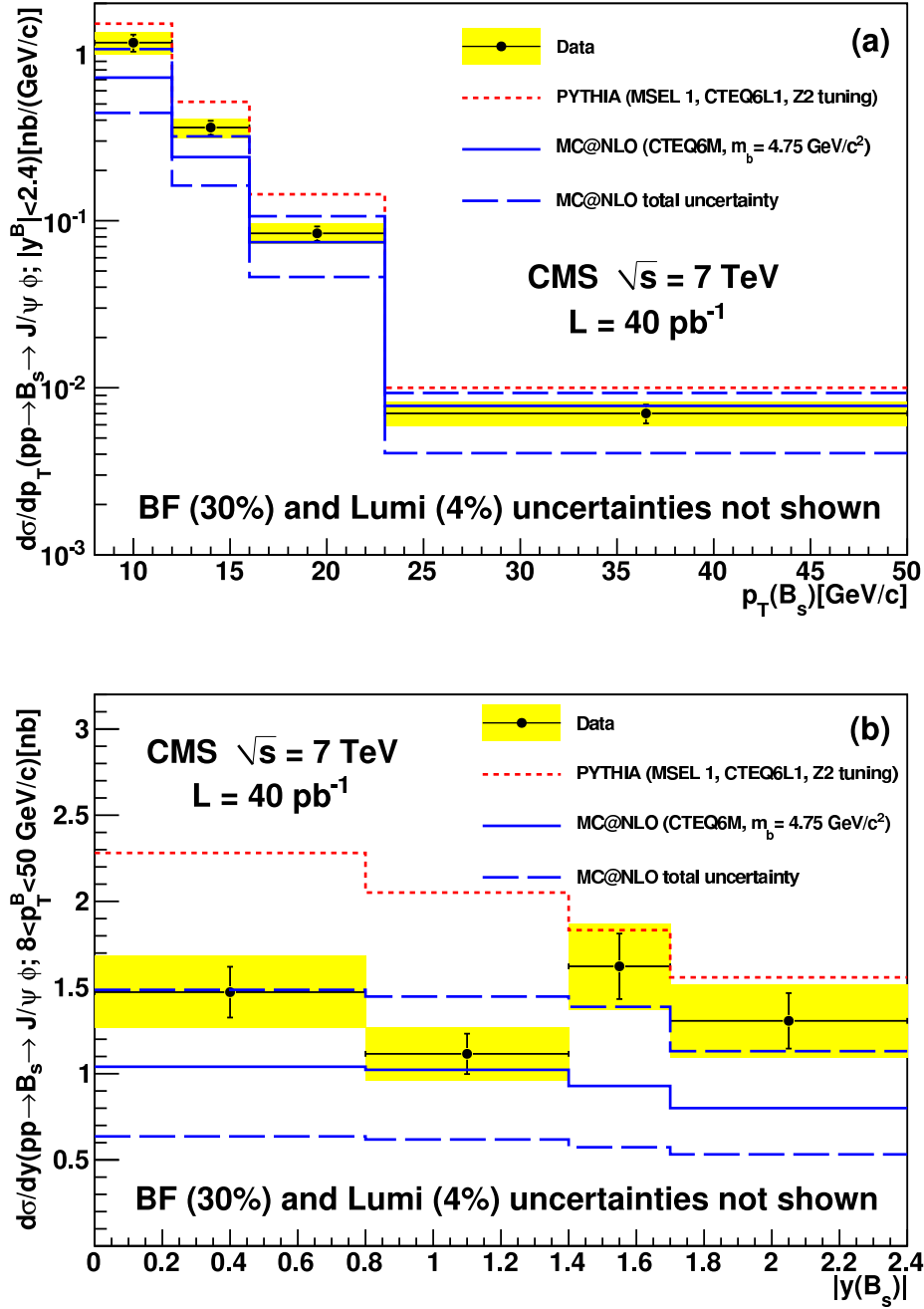


Figure 2: Measured differential cross sections  $d\sigma/dp_T^B$  (a) and  $d\sigma/dy^B$  (b) compared with theoretical predictions. The (yellow) band represents the sum in quadrature of statistical and systematic uncertainties. The dotted (red) line is the PYTHIA prediction; the solid and dashed (blue) lines are the MC@NLO prediction and its uncertainty, respectively. The common uncertainties of 4% on the data points, due to the integrated luminosity, and of 30% on the theory curves, due to the  $B_s^0 \rightarrow J/\psi \phi$  branching fraction, are not shown.

## References

- 1 P. Nason et al., “The Total Cross-Section for the Production of Heavy Quarks in Hadronic Collisions”, *Nucl. Phys. B* **303** (1988) 607.
- 2 CDF Collaboration, “Measurement of the bottom quark production cross-section using semileptonic decay electrons in  $p\bar{p}$  collisions at  $\sqrt{s} = 1.8$  TeV”, *Phys. Rev. Lett.* **71** (1993) 500.
- 3 CDF Collaboration, “Measurement of the  $B$  meson differential cross-section,  $d\sigma/dp_T$ , in  $p\bar{p}$  collisions at  $\sqrt{s} = 1.8$  TeV”, *Phys. Rev. Lett.* **75** (1995) 1451.
- 4 CDF Collaboration, “Measurement of the  $B^+$  total cross section and  $B^+$  differential cross section  $d\sigma/dp_T$  in  $p\bar{p}$  collisions at  $\sqrt{s} = 1.8$  TeV”, *Phys. Rev. D* **65** (2002) 052005.
- 5 D0 Collaboration, “Inclusive  $\mu$  and  $b$ -quark Production Cross Sections in  $p\bar{p}$  Collisions at  $\sqrt{s} = 1.8$  TeV”, *Phys. Rev. Lett.* **74** (1995) 3548.
- 6 D0 Collaboration, “Small angle muon and bottom quark production in  $p\bar{p}$  collisions at  $\sqrt{s} = 1.8$  TeV”, *Phys. Rev. Lett.* **84** (2000) 5478.
- 7 D0 Collaboration, “Cross section for  $b$  jet production in  $p\bar{p}$  collisions at  $\sqrt{s} = 1.8$  TeV”, *Phys. Rev. Lett.* **85** (2000) 5068.
- 8 CDF Collaboration, “Measurement of the  $J/\psi$  meson and  $b$ -hadron production cross sections in  $p\bar{p}$  collisions at  $\sqrt{s} = 1960$  GeV”, *Phys. Rev. D* **71** (2005) 032001.
- 9 CDF Collaboration, “Measurement of the  $B^+$  production cross section in  $p\bar{p}$  collisions at  $\sqrt{s} = 1960$  GeV”, *Phys. Rev. D* **75** (2007) 012010.
- 10 M. Cacciari et al., “QCD analysis of first  $b$  cross-section data at 1.96 TeV”, *JHEP* **07** (2004) 033.
- 11 M. Cacciari et al., “The  $p_T$  spectrum in heavy-flavour hadroproduction”, *JHEP* **05** (1998) 007.
- 12 B. A. Kniehl et al., “Finite-mass effects on inclusive  $B$ -meson hadroproduction”, *Phys. Rev. D* **77** (2008) 014011.
- 13 LHCb Collaboration, “Measurement of  $\sigma(pp \rightarrow b\bar{b}X)$  at  $\sqrt{s} = 7$  TeV in the forward region”, *Phys. Lett. B* **694** (2010) 209.
- 14 CMS Collaboration, “Measurement of the  $B^+$  production cross section in  $pp$  collisions at  $\sqrt{s} = 7$  TeV”, *Phys. Rev. Lett.* **106** (2011) 112001.
- 15 CMS Collaboration, “Measurement of the  $B^0$  production cross section in  $pp$  collisions at  $\sqrt{s} = 7$  TeV”, *Phys. Rev. Lett.* **106** (2011) 252001.
- 16 CMS Collaboration, “The CMS experiment at the CERN LHC”, *JINST* **0803** (2008) S08004.
- 17 CMS Collaboration, “Vertex Fitting in the CMS Tracker”, *CMS Analysis Note* **CMS-AN-06-032** (2006).
- 18 Particle Data Group Collaboration, “Review of particle physics”, *J. Phys.* **G37** (2010) 075021.
- 19 CMS Collaboration, “Prompt and non-prompt  $J/\psi$  production in  $pp$  collisions at  $\sqrt{s} = 7$  TeV”, *Eur. Phys. J. D* **71** (2011) 1575.
- 20 K. Prokofiev and T. Speer, “A kinematic and a decay chain reconstruction library”, in *Proceedings of Computing in High Energy Physics and Nuclear Physics*, p. 411. Interlaken, Switzerland, September, 2004.
- 21 CMS Collaboration, “Tracking and Primary Vertex Results in First 7TeV Collisions”, *CMS Physics Analysis Summary* **CMS-PAS-TRK-10-005** (2010).
- 22 T. Sjöstrand et al., “PYTHIA 6.4 physics and manual”, *JHEP* **05** (2006) 026.
- 23 D. J. Lange, “The EvtGen particle decay simulation package”, *Nucl. Instrum. Meth. A* **462** (2001) 152.
- 24 GEANT4 Collaboration, “GEANT4: A simulation toolkit”, *Nucl. Instrum. Meth. A* **506** (2003) 250.
- 25 CMS Collaboration, “Measurement of Tracking Efficiency”, *CMS Physics Analysis Summary* **CMS-PAS-TRK-10-002** (2010).
- 26 I. Antcheva et al., “ROOT – A C++ framework for petabyte data storage, statistical analysis and visualization”, *Comput. Phys. Commun.* **180** (2009) 2499.
- 27 S. Frixione et al., “Matching NLO QCD and parton showers in heavy flavour production”, *JHEP* **08** (2003) 007.
- 28 CMS Collaboration, “Measurement of CMS Luminosity”, *CMS Physics Analysis Summary* **CMS-PAS-EWK-10-004** (2010).
- 29 J. Pumplin et al., “New generation of parton distributions with uncertainties from global QCD analysis”, *JHEP* **07** (2002) 012.
- 30 R. Field, “Early LHC Underlying Event Data–Findings and Surprises”, in *Proceedings of the Hadron Collider Physics Symposium*. 2010.
- 31 CMS Collaboration, “Measurement of the Strange  $B$  Meson Production Cross Section with  $J/\psi\phi$  Decays in  $pp$  Collisions at  $\sqrt{s} = 7$  TeV”, (Accepted by *Phys. Rev. D - Rapid Communication*) (2011).